Journal of Composite Materials
http://jcm.sagepub.com/

Characterizing Mechanical Properties of Particulate Nanocomposites Using Micromechanical Approach

Jia-Lin Tsai and Shi-Hua Tzeng

Journal of Composite Materials 2008 42: 2345 originally published online 7 August 2008
DOI: 10.1177/0021998308095503

The online version of this article can be found at:
http://jcm.sagepub.com/content/42/22/2345

Published by:
SAGE
http://www.sagepublications.com

On behalf of:
American Society for Composites

Characterizing Mechanical Properties of Particulate Nanocomposites Using Micromechanical Approach

JIA-LIN TSAI* AND SHI-HUA TZENG
Department of Mechanical Engineering
National Chiao Tung University, Hsinchu, Taiwan 300, ROC

ABSTRACT: This research aims to propose a continuous micromechanical model for characterizing the mechanical properties of the nanocomposites containing silica nanoparticles embedded in polyimide matrix. The molecular structures of the nanocomposites were established through molecular dynamic (MD) simulation, from which the non-bonded gap as well as the non-bonded energy between the nano-sized inclusion and the surrounding matrix were evaluated. It was postulated that the normalized non-bonded energy (non-bonded energy divided by surface area of the inclusion) is correlated with the degree of interfacial interaction. Subsequently, an effective interphase micromechanical model including inclusion, matrix and effective interphase was developed, in which the dimension of the effective interphase was assumed equal to the non-bonded gap and the corresponding elastic stiffness was calculated from the normalized non-bonded energy. Comparison of the results calculated from the micromechanical model and the MD simulation indicates that the effective interphase model is capable of describing Young's modulus of particulate nanocomposites with accuracy. In addition, it was revealed that when the particulate size decreases, the corresponding modulus of the nanocomposites increases.

KEY WORDS: nanocomposites, MD simulation, micromechanical model, Young's modulus.

INTRODUCTION

WITH EXTENSIVE APPLICATIONS of polymer and its composites, the demand for the materials possessing the characteristics of high stiffness and strength is increasing. In order to improve mechanical properties, spherical particles have been used as reinforcement in polymeric materials for many years. In general, these composite materials were reinforced with micron-sized inclusions. However, with the advance of the nanotechnology as well as the processing techniques, various types of particles with nanoscale have been developed and then dispersed into conventional polymeric material

*Author to whom correspondence should be addressed. E-mail: jialin@mail.nctu.edu.tw
Figure 1 appears in color online: http://jcm.sagepub.com

0021-9983/08/22 2345–17 $10.00/0 DOI: 10.1177/0021998308095503

to form the nanocomposites. It is interesting to note that from a continuous micromechanics point of view, the spherical particle size basically has no significant effect on the mechanical properties of its composites if the particle volume fraction remains the same. However, several researchers recently investigated the particle size effect on the mechanical behaviors of composites, indicating that to some extent, the particle size may influence the responses of composites, which is not in agreement with the expectations using continuum mechanics. Among the investigations, some experimental data showed that because of the increase of the surface area, the mechanical properties of the composites increase as the particle sizes decrease [1–6]. On the other hand, there are other results demonstrating no size effect or reverse tendency [7,8]. So far, no definite conclusions have been achieved.

Chen and Sun [1] introduced hydroxyapatite (HA) particles into poly(ε-caprolactone) (PCL) to form conventional composites. Two different micron sizes of HA particles, 3–8 and 20–80 μm were considered in their studies. Although the reinforcements was not in nanoscale, it was revealed that the HA with smaller particle size, because of its large surface area, exhibits greater improvement in yield strength, tensile modulus, storage modulus and loss modulus. Chisholm et al. [2] investigated the mechanical and thermal properties of the epoxy system infused with micro- and nano-sized SiC fillers, respectively. They found that the nano fillers could provide better stiffness, strength and thermal properties to the matrix than its counterpart. The enhancing mechanism could be attributed to the increasing extent of cross-linking within the polymer matrix caused by the presence of the nano-particles as a role of catalyst. Vollenberg et al. [3,4] investigated the surface treatment effect in conjunction with the particulate size effect on the behavior of the composites. It was revealed that for the silane-treated glass beads inclusion, Young's modulus is not influenced by the particle size of the fillers. However, when the surfaces of the glass bead fillers were not treated with any surfactant, the modulus seems dramatically dependent on the particle size. It is noted that in their experiment, the filler sizes are still within the micron ranges. Cho et al. [5] introduced glass beads and aluminum oxide particles with sizes ranging from 0.5 mm to 15 nm as spherical fillers infused into vinyl ester polymer. It was demonstrated that Young's modulus of the composites is independent of the particle size when the particle is in the micron range. Nevertheless, when the filler sizes are within the nanoscale, the composite modulus increases with the decreasing of particle size. Ng et al. [6] used nano- and micron-TiO_2 particles as fillers in diglycidyl ether bisphenol A (DGEBA) epoxy system pointing out that the nanocomposites exhibit superior combined properties, such as higher modulus, higher failure stress, and larger strain to failure as compared to the conventional micro-composites. Reynaud et al. [7] investigated the behaviors of polyamide 6 (PA6) nano-composite reinforced by silica spherical particles with three different diameters: 17, 30, and 80 nm. It was found that the filler diameter basically has no effect on the modulus of the nanocomposites. The size effect of the calcium carbonate on the ABS polymer system was investigated by Jiang et al., and the results demonstrated that the composites with micron-size filler exhibit higher modulus than the nanocomposites with nanosize fillers [8]. Apparently, the observation is quite different from the results performed by other researchers [2,5,6]. When the inorganic fillers are introduced into organic matrix system, many factors, including filler morphology, size, amount, surface treatment, and the dispersion homogeneity, could extensively influence the composite performance. Sometimes these factors could form couple effects that may further complicate the problem. Therefore, from an experimental point of view, it is still a challenging task to identify a specific mechanism that could depict the inclusion size effect

on the mechanical behaviors of the composites. A comprehensive review on the behaviors of polymer nanocomposites was found in the literature provided by Jordan et al. [9].

In light of the aforementioned difficulty, several researchers attempted to characterize the mechanical behaviors of the particulate nanocomposites using a numerical simulation to understand the deep insight of mechanics of nanocomposites [10–12]. Odegard et al. conducted molecular simulation to characterize the interface interaction between the nanoparticles and surrounding polyimide matrix with various particle surface treatment and particle size [10]. A micromechanical model with effective interphase was proposed to model the properties of the nanocomposites. Results demonstrated that when the particle sizes increase, the modulus of the nanocomposites increase accordingly. However, in their analysis, the thickness of the effective interface as well as its properties was not specified clearly. Cannillo et al. [11] modeled the silica particles filled in the PCL (polycaprolactone) matrix using a FEM model. By introducing a third phase, namely the interphase, around the particle in the micromechanics analysis, they accurately predicted the mechanical properties of the nanocomposites with various amount of particle loading. In their analysis, it was hypothesized that the dimension of the interphase is the same as the average particle radius, and the modulus of the interphase is set equal to the average value of the modulus of the particles and matrix. Avella et al. [12] adopted the same manner with the interphase of about 100 nm to model the PCL/silica nanocomposites. Because nano-inclusion provides a very high specific surface area as compared to the micro-particle, the thickness as well as the modulus of the interphase surrounding the nano-inclusion may be expected to play an important role in the nanocomposite's overall behaviors [13,14]. Moreover, the other behaviors such as the crack propagation are also influenced by the nanoparticles as well as their interfacial adhesion to the surrounding polymers [15]. Therefore, a more complete model, including the interfacial effect, is required to describe the properties of the nanocomposites with accuracy. In particular, the thickness of the effective interphase layer and its associated properties have to be properly determined [16].

This object of the research is to propose a continuum-based micromechanical model, including spherical inclusion, matrix and effective interface, for describing the mechanical properties of silica/polyimide nanocomposites. The molecular dynamic (MD) simulation was performed to build an equilibrated molecular structure of the nanocomposites, based on which the effective interphase and its properties were determined. With the interphase properties, the behaviors of the nanocomposites were characterized using the continuum mechanical model. Meanwhile, the particle size effect on the behavior of the nanocomposites will also be examined in this study.

GENERATION OF MOLECULAR STRUCTURES

The molecular structure of silica/polyimide nanocomposites suitable for molecular dynamic simulation was constructed at the beginning of the research. A representative volume element (RVE) as shown in Figure 1 with periodicity boundary conditions containing a spherical silica particle embedded in the amorphous polyimide molecular chains was constructed to represent the particulate nanocomposites. In the above molecular model, the particles were assumed to disperse regularly and homogeneously within the polyimide matrix. To generate the spherical nano-particles shown in Figure 1, an α type silica crystal was created initially, and all Si and O atoms with the radius measured from the sphere center greater than a certain value were then discarded.

While the polyimide polymer was generated by several molecular chains, depending on the size of the RVE and each molecular chain contains 10 repeated units. Figure 2 illustrates the polyimide monomer unit. It should be noted that the polyimide chains were generated randomly with covalent bonding between adjacent atoms and the initial dimensions of the RVE were adjusted such that the density of the polyimide is close to the experimentally measured value of 1.31 g/cm^3 [17]. Once the dimensions of the RVE were decided, the initial configuration of the nanocomposites was constructed by positing the spherical particle into the center of the RVE followed by generating the molecular chains in the remaining space. There are four different particulate sizes, 6.29, 8.50, 11.56, and 13.45 Å in radius, which were considered in the simulation.

Subsequently, the force field used for describing the atom/molecular interactions needed to be specified in the MD simulation. In this study, the compass force field derived based on *ab initio* calculation was selected to characterize the silica particles and the polyimide polymer as well as their reciprocal interactions. Having consolidated coverage of organic and inorganic materials, the compass force field is applicable for treating the non-bonded interaction between the silica and the polyimide polymers [18,19]. It is noted that for the inorganic materials, the parameterization and validation of the compass force field were conducted based on the energy minimization at zero temperature, resulting in that the

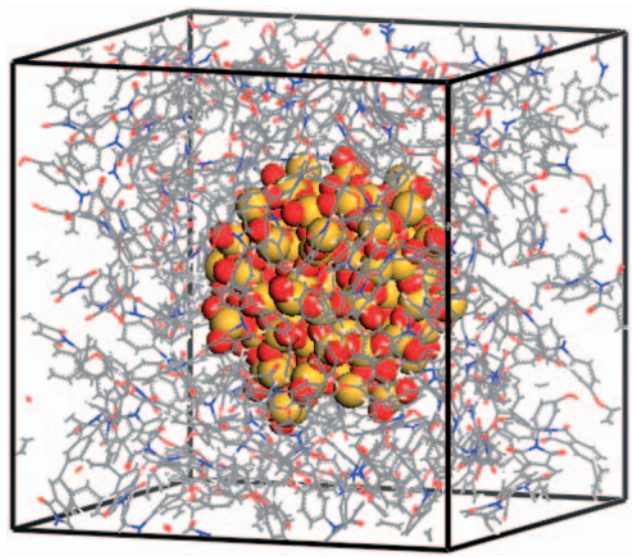

Figure 1. *Representative volume element of the particulate nanocomposites.*

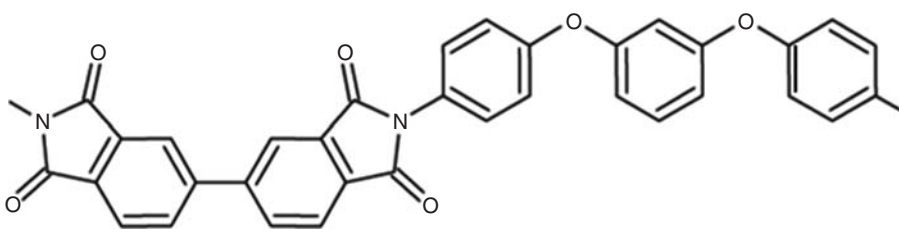

Figure 2. *Schematic of polyimide monomer unit.*

temperature effect were not taken into account in their corroboration. Therefore, in the following MD simulation, the molecular structure of the nanocomposites and their associated properties were equilibrated and calculated at zero temperature condition.

The MD simulations were conducted using Material Studio package (4.0 version) provided by Accelrys Inc. [18]. During the simulation, the equilibrated molecular structure with minimized energy was first accomplished, and afterward, the structure was subjected to displacement fields in the three different directions for evaluating the corresponding mechanical properties. In order to build an equilibrated molecular structure suitable for silica/polyimide nanocomposites, the NVT and NPT ensembles were employed sequentially in the MD simulation. Here, the NVT ensemble stands for that the volume and temperature is fixed during the simulation; however, the NPT ensemble represents the fixed pressure and temperature variables. The purpose of the NVT ensemble conducted at 1500 K for 80 ps was to supply enough kinetic energy on the molecular atoms so that homogeneous molecular structure within the RVE can be achieved. The NPT process was designated to 0 atm such that the RVE with traction-free boundary conditions can be satisfied. Because the compass force field employed for the inorganic materials is validated only at zero temperature, the temperature in the NPT ensemble was eventually set at 0 K. Two sub-steps were introduced for the temperature decreasing in the NPT process. In the first step, the temperature was designated at 300 K for 60 ps, and the following step was appointed at 0 K for 80 ps. During the simulation, the total potential energy variation was examined, and when the quantity fluctuated around a certain mean value for a while, the system was considered as equilibrium. Figures 3 and 4 demonstrate the energy history of the nanocomposites as well as the temperature variation during the second step in the NPT simulation, respectively. It seems that the potential energy attains stable condition after 80 ps, and meanwhile, the kinetic energy is approaching zero. Based on the observations, it was suggested that the current molecular structure is in the equilibrium condition and suitable for the characterization of the material constants.

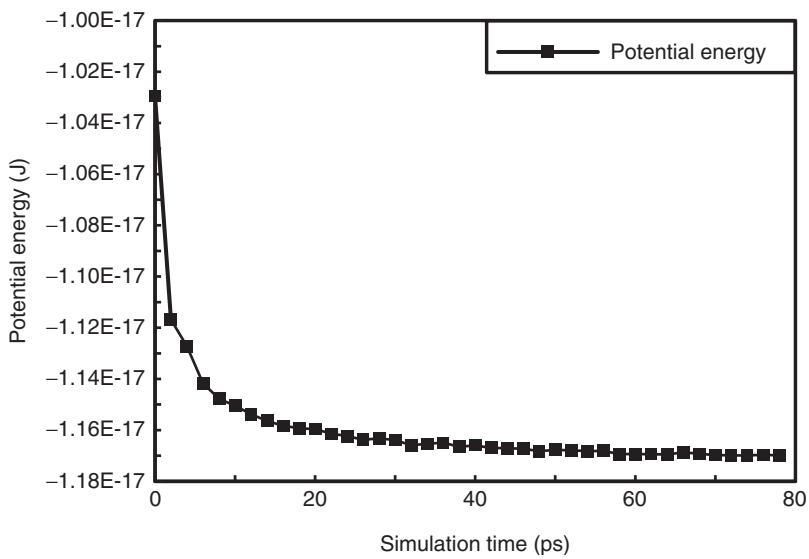

Figure 3. *Variation of potential energy in NPT ensemble.*

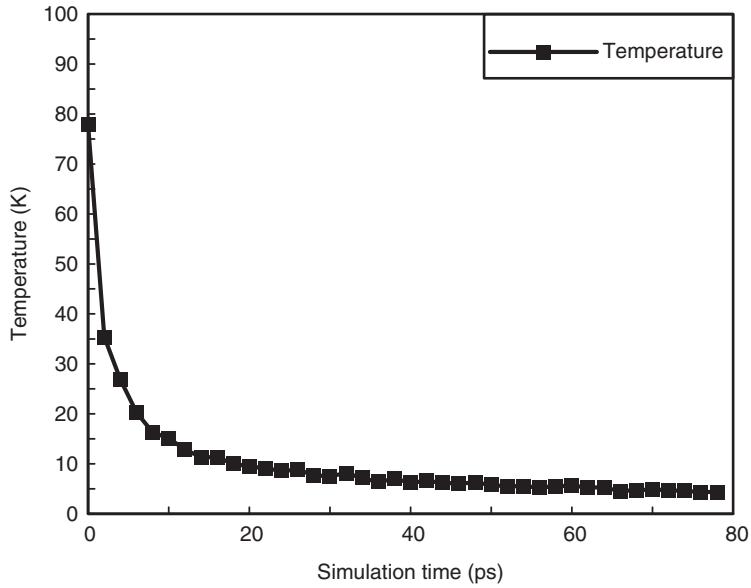

Figure 4. *Variation of temperature in NPT ensemble.*

NON-BONDED GAP AND NON-BONDED ENERGY

Figure 5 illustrates the density distribution of the silica and the PI polymer in the radial direction. It can be seen that near the silica particle, the polyimide density is higher, and it then declines to a typical value when it is far away. In addition, there is clear gap with relatively lower molecular density existing between the silica particle and the surrounding polyimide matrix. In this study, the gap was referred to as the non-bonded gap because it is caused by the non-bonded force field between the nanoparticle and the polymeric matrix. In order to qualitatively characterize the dimension of the non-bonded gap, two radial lines, emitted from the center of the particle with a small angle difference $\Delta\phi$, were rotated with respected to the z-axis. For each rotating increment $\Delta\theta$, a radial volume element as shown in Figure 6 was created where a numbers of silica and polyimide atoms were counted. The maximum radial distance for the silica atoms in the volume element is denoted as $r_{\mathrm{SiO_2}}^{\max}$, and the minimum radial distance for the polyimide atoms is represented as $r_{PI}^{\min}$. The non-bonded gap between the silica particle and the polyimide matrix within the unit volume is introduced as:

$$r_{\text{non-bonded}} = r_{\mathrm{PI}}^{\min} - r_{\mathrm{SiO_2}}^{\max}. \tag{1}$$

Figure 7 illustrates the measurements of the maximum radial distance for silica atoms together with the minimum radial distance for polyimide atoms for each $\Delta\theta$ increment. When the radial volume element rotates around 360°, the average value of the $r_{\text{non-bonded}}$ is regarded as the non-bonded gap of the nanocomposites. Table 1 indicates the non-bonded gap calculated from the nanocomposites with four different particle sizes. It was found that the non-bonded gap increases as the particle size increases. However, in this regard, the dependence of non-bonded gap on the particle size is not significant.

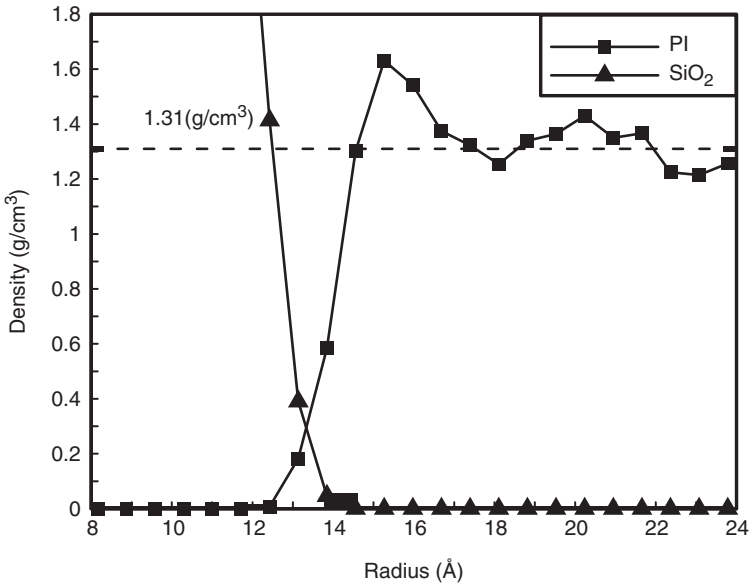

Figure 5. *Density distributions of the silica and polyimide in the radial direction.*

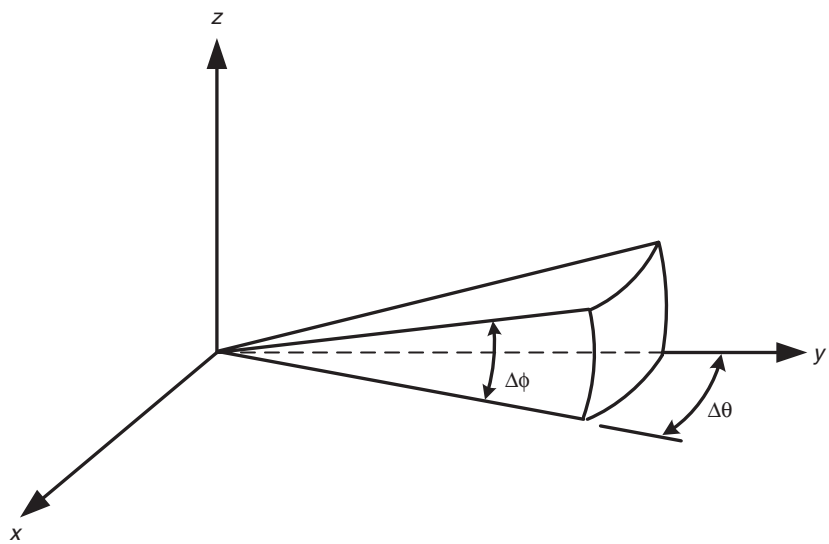

Figure 6. *Determination of radial volume element for the non-bonded gap.*

In addition to the non-bonded gap the non-bonding energy between the nanoparticle and the polyimide matrix was also estimated from the MD simulation. In the compass force field, the non-bonded interaction consists of the electrostatic and van der Waals interactions that are modeled by the Coulomb function and Lennard–Jones function, respectively. It is noted that, in reality, some kind of cross-linking between particulate and matrix may be constructed in the curing process. This phenomenon was not considered in the present modeling. The total non-bonded energy within the nanocomposites is

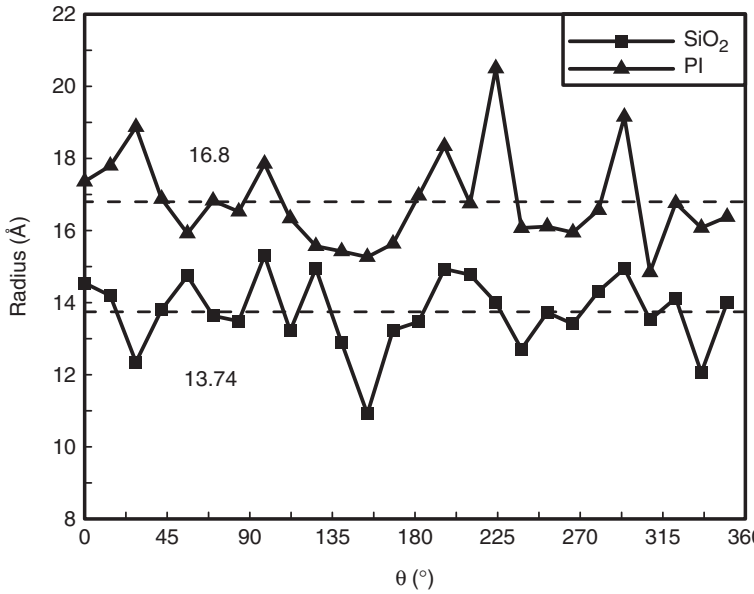

Figure 7. *Measurements of the maximum radial distance for silica atoms and the minimum radial distance for polyimide atoms within each radial volume element.*

Table 1. Non-bonded gap for the silica/polyimide nanocomposites with four different inclusion sizes.

Nanocomposites	PI-SiO_2	PI-SiO_2	PI-SiO_2	PI-SiO_2
Particle radius (Å)	6.29	8.50	11.56	13.45
Non-bond gap (Å)	4.06	3.99	3.26	3.24

contributed not only by the interaction between the nanoparticle and the polyimide but also by the silica nanoparticle itself as well as the polyimide molecular chains. Therefore, the non-bonded energy between the silica and polyimide interface is calculated by subtracting the non-bonded energy of the particle and polymer from the total non-bonded energy, and it is written as:

$$U_{\mathrm{PI-silica}} = U_{\mathrm{total}} - U_{\mathrm{silica}} - U_{\mathrm{PI}} \tag{2}$$

where U_{total} is the total non-bonded energy obtained from the overall nanocomposites. U_{silica} and U_{PI} stand for the non-bonded energy of silica particle and polyimide molecular chain, respectively. The non-bonded energy of the polyimide molecular chain was evaluated in the RVE when the nanoparticle was removed, and only the molecular structures of the polyimide matrix were left. In a similar manner, the non-bonded energy of silica was calculated. Therefore, with Equation (2), the non-bonded energy between the nanoparticles and the polyimide was determined. It is worthy to note that the non-bonded energy provides an indication regarding the extent of interaction between the particle and the surrounding matrix. If the non-bond interaction can be further employed to represent

the characteristics of an equivalent interphase with the dimension equal to the non-bond gap, it is possible that the mechanical properties of the nanocomposites could be described by a continuum micromechanical model.

To achieve this goal the degree of interaction between the particle and the matrix is characterized in terms of the normalized non-bonded energy, which is defined as the non-bonded energy divided by the surface area of the spherical particle. Subsequently, the normalized non-bonded energy was assumed to be associated with the non-bonded gap in the form of:

$$U(r) = \frac{1}{6}kr^6 \tag{3}$$

where r is the non-bonded gap, and k is the parameter to be determined. Based on the normalized non-bonded energy, the corresponding normalized interaction force was obtained by differentiating the energy with respect to the distance as:

$$F(r) = -\frac{\partial U}{\partial r} = -kr^5. \tag{4}$$

The negative sign of the force in Equation (4) represents the attractive interaction. On the other hand, Equations (3) and (4) can also be interpreted as the strain energy of a unit element with length equal to the non-bond gap, r, and cross-section equal to one when it is subjected to the applied loading kr^5. Therefore, from the 1-D elasticity, the strain energy of the unit element is represented as:

$$U = \frac{\sigma^2}{2E}r \tag{5}$$

where E is Young's modulus of the equivalent unit element, and σ is equal to kr^5 that is the loading applied on the unit area (so-called stress). From the hypothesis that the strain energy of the unit element is equivalent to the normalized energy given in Equation (3), the modulus of the equivalent unit element is yielded as:

$$E = 3kr^5 = \frac{18U(r)}{r}. \tag{6}$$

It is noted that in the above calculation, only the strain energy caused by axial loading was considered to illustrate the normalized strain energy of the nanocomposites obtained from the MD simulation. As a result, once the non-bonded gap as well as the normalized non-bonded energy was calculated, the elastic modulus of the equivalent interphase can be determined by means of Equation (6). Figure 8 demonstrates the normalized non-bonded energy of the nanocomposites calculated with different particle sizes. It shows that as the particle size decreases, the corresponding normalized non-bonded energy increases, and the interaction is intensified.

Based on the aforementioned derivation, the non-bonded interaction between the reinforced particle and the surrounding matrix can be appropriately replicated by a continuum-equivalent interphase. With the mechanical properties of the interphase in combination with the properties of spherical particle and surround polymer, the

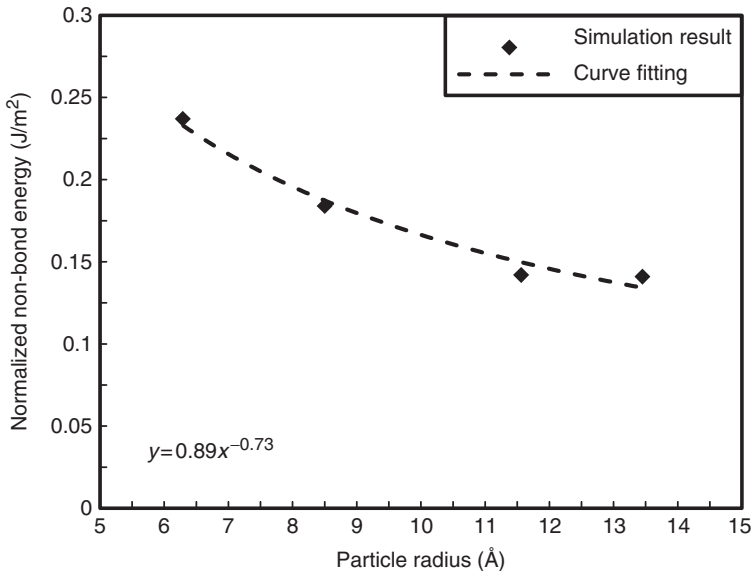

Figure 8. *Particle size effect on the normalized non-bonded energy of silica/polyimide nanocomposites.*

mechanical properties of the nanocomposites can be predicted using the continuum micromechanical model. It is noted in the following analysis that Poisson's ratio of the interphase is assumed to be 0.3.

EFFECTIVE INTERPHASE MODEL

When the mechanical properties of the particle, interphase, and matrix as well as the corresponding geometric parameters were determined, the behaviors of the nanocomposites can be depicted using the micromechanical model with multiphase particles [20,21]. It should be noted that three ingredients were considered in the effective interphase model, which is different from conventional Mori–Tanaka micromechanical model [22] where only two phases were included in the analysis. The explicit formulation of the effective interphase model is written as [21]:

$$C^* = C^m + \left[(v_\Gamma + v_\Omega)\{C^\Gamma - C^m\}A_V^{di} + v_\Omega\{(C^\Omega - C^\Gamma)A_\Omega^{di}\}\right]\left[v_m I + (v_\Gamma + v_\Omega)\{A_V^{di}\}\right]^{-1} \quad (7)$$

where C^* denoted the stiffness matrix for the nanocomposites. C^Ω, C^Γ, and C^m represent the stiffness of the domain of Ω (inclusion), Γ (interphase) and m (matrix), respectively as shown in Figure 9, and v_Ω, v_Γ, and v_m indicate the volume friction of the respective domains. In addition:

$$A_\Gamma^{di} = I + \left(E_{Esh}^V \frac{v_\Omega}{v_\Gamma}\Delta E\right)\Phi^\Gamma + \frac{v_\Omega}{v_\Gamma}\Delta E\Phi^\Omega \quad (8)$$

$$A_V^{di} = I + E_{Esh}^V \Phi^V \quad (9)$$

$$A_\Omega^{di} = I + \Delta E_{Esh}\Phi^\Gamma + E_{Esh}^\Omega \Phi^\Omega \quad (10)$$

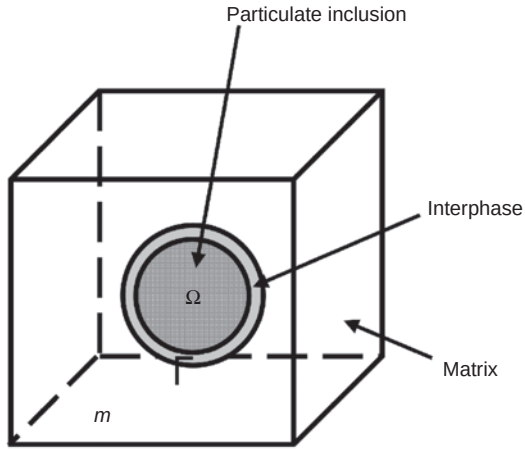

Figure 9. *Schematic of effective interphase model.*

where

$$\Phi^{\Omega} = -\left[(E^{\Omega}_{Esh} + C^{1}) + \Delta E_{Esh}(E^{\Omega}_{Esh} - \frac{v_{\Omega}}{v_{\Gamma}}\Delta E_{Esh} + C^{2})^{-1}(E^{\Omega}_{Esh} - \frac{v_{\Omega}}{v_{\Gamma}}\Delta E_{Esh} + C^{1})\right]^{-1} \tag{11}$$

$$\Phi^{V} = \frac{v_{\Omega}}{v_{\Omega} + v_{\Gamma}}\Phi^{\Omega} + \frac{v_{\Gamma}}{v_{\Omega} + v_{\Gamma}}\Phi^{\Gamma} \tag{12}$$

$$\Phi^{\Gamma} = -\left[\Delta E_{Esh} + (E^{\Omega}_{Esh} + C^{1})(E^{\Omega}_{Esh} - \frac{v_{\Omega}}{v_{\Gamma}}\Delta E_{Esh} + C^{1})^{-1}(E^{\Omega}_{Esh} - \frac{v_{\Omega}}{v_{\Gamma}}\Delta E_{Esh} + C^{2})\right]^{-1} \tag{13}$$

$$\Delta E_{Esh} = E^{\Omega}_{Esh} - E^{V}_{Esh} \tag{14}$$

$$C^{1} = (C^{\Omega} - C^{m})^{-1}C^{m} \tag{15}$$

$$C^{2} = (C^{\Gamma} - C^{m})^{-1}C^{m}. \tag{16}$$

In the above expression, $V = \Omega + \Gamma$, which is the domain comprising the particulate inclusion and the interphase as well, and E^{V}_{Esh} and E^{Ω}_{Esh} indicate the Eshelby's tensor for the domains V and Ω, respectively [23]. It is noted that when the aspect ratio of the inclusion phases are equal to one, such as spherical particle, the Eshelby's tensors can be written explicitly as [24]:

$$E^{\Omega}_{Esh} = E^{V}_{Esh} = E_{ijkl} \tag{17}$$

where

$$E_{1111} = E_{2222} = E_{3333} = \frac{7 - 5\nu_m}{15(1 - \nu_m)} \tag{18}$$

$$E_{1122} = E_{2233} = E_{3311} = E_{1133} = E_{2211} = E_{3322} = \frac{5\nu_m - 1}{15(\nu_m - 1)} \tag{19}$$

$$E_{1212} = E_{2323} = E_{3131} = \frac{4 - 5\nu_m}{15(1 - \nu_m)} \tag{20}$$

and ν_m is Poisson's ratio of the surrounding matrix.

In the above micromechanical model, all three phases are assumed to be perfectly bonded together, although there is a non-bonded gap existing between the spherical particle and the surrounding matrix. The interaction between the non-bonded gaps was modeled as an effective interphase, the corresponding properties of which were derived from the normalized non-bonded energy calculated using molecular simulation as described earlier. As a result, with the properties of the inclusion, matrix and the effective interphase, the associated behavior of the nanocomposites can be predicted using Equation (7). In this approach, it was suggested that the discreet molecular structure of nanocomposites could be converted into a continuum system, and the corresponding properties could be simulated using the continuum micromechanical analysis when the equivalent interphase properties were properly determined.

ELASTIC CONSTANTS OF MOLECULAR STRUCTURES

In addition to the micromechanical analysis discussed previously, the mechanical properties of the equilibrated molecular configuration of nanocomposites can also be predicted using the molecular simulation [25]. By applying a small amount of strain component on the RVE, while the other strain components are remaining at zero, the deformed state of the molecular structure was produced. Once the equilibrium condition was accomplished in the deformed state, the associated stress was then calculated from the virial theorem [26], and the stiffness matrix C_{ij} of the nanocomposites was measured as the derivative of the stress associated with the corresponding strain component

$$C_{ij} = \frac{\Delta\sigma_i}{\Delta\varepsilon_j}. \tag{21}$$

where the stress components σ_{ij} is expressed as:

$$\sigma = -\frac{1}{V_0}\left(\sum_{i<j} r_{ij} f_{ij}^T\right). \tag{22}$$

In Equation (22) r_{ij} and f_{ij} denotes the atomic distance and the corresponding interaction force between any two atoms within the cut-off distance. V_o represents the total volume of the RVE. It is noted that in Equation (22), because the model was simulated at 0 K, the temperature effect was neglected in the stress computation. With a microstructures of RVE given in Figure 1, the nanocomposites were assumed to be cubic symmetric. For a cubic symmetric material, the stiffness matrix C_{ij} can be expressed explicitly as:

$$[C] = \begin{bmatrix} C_{11} & C_{12} & C_{13} & 0 & 0 & 0 \\ C_{12} & C_{22} & C_{23} & 0 & 0 & 0 \\ C_{13} & C_{23} & C_{33} & 0 & 0 & 0 \\ 0 & 0 & 0 & C_{44} & 0 & 0 \\ 0 & 0 & 0 & 0 & C_{55} & 0 \\ 0 & 0 & 0 & 0 & 0 & C_{66} \end{bmatrix} \tag{23}$$

where $C_{11} = C_{22} = C_{33}$; $C_{44} = C_{55} = C_{66}$; and $C_{12} = C_{13} = C_{23}$, and thus, there are only three independent elastic constants existing in the stiffness matrix. In theory, the above relations should be satisfied if the microstructure of the nanocomposites is periodic, and all ingredient properties are homogeneous and isotropic. However, in the molecular simulation, it is difficult to construct such a homogeneous molecular structure that the values of C_{11}, C_{22}, and C_{33} in the stiffness matrix are the same, and the values of C_{12}, C_{13}, and C_{23} are the same as well. The discrepancy of C_{11}, C_{22}, and C_{33} may be regarded as an index for the extent of homogeneity of the molecular structure and are used to validate the applicability of the molecular model to characterize the mechanical properties of nanocomposites. Table 2 shows C_{11}, C_{22}, and C_{33} as well as C_{12}, C_{13}, and C_{23} values obtained from the molecular simulation with four different sizes of spherical inclusions. It seems that the variations are quite small (less than 10%); therefore the current molecular models were believed to be suitable for describing the mechanical properties of the nanocomposites. In order to calculate the Young's modulus of the nanocomposites using the cubic symmetric concept, the averaged ones of the elements were employed, and the modulus is derived as [27]:

$$E_{11} = \bar{C}_{11}\left(1 - \frac{2\bar{C}_{12}^2}{\bar{C}_{11}(\bar{C}_{11} + \bar{C}_{12})}\right) \tag{24}$$

where $\bar{C}_{11} = \frac{1}{3}(C_{11} + C_{22} + C_{33})$ and $\bar{C}_{12} = \frac{1}{3}(C_{12} + C_{13} + C_{23})$. The modulus derived using the above molecular approach will be compared to those calculated from continuum-based micromechanical model. It should be noted that the material properties of ingredients, i.e., silica and polyimide, were also determined using the molecular simulation as described before and the results are summarized in Table 3. The material constants were then employed in the continuum micromechanical model together with the interphase properties for characterizing the mechanical behaviors of the particulate nanocomposites.

Table 2. The elements in the stiffness matrix for the silica/polyimide nanocomposites calculated from MD simulation.

Particle radius (Å)	6.29	8.50	11.56	13.45
C_{11}(GPa)	8.87	8.26	9.12	8.34
C_{22}(GPa)	9.22	8.08	9.02	9.00
C_{33}(GPa)	8.44	9.07	8.93	8.85
C_{12}(GPa)	5.5	5.5	5.8	5.6
C_{13}(GPa)	5.5	5.2	6.2	5.9
C_{23}(GPa)	5.7	5.3	5.7	5.6

Table 3. Material properties of silica and polyimide used in the micromechanical simulation of nanocomposites.

	Silica	**Polyimide**
Young's modulus (GPa)	84	3.68
Poisson's ratio	0.11	0.38

Table 4. Comparison of the modulus of the silica/polyimide nanocomposites calculated using effective interphase model, MD simulation and Mori–Tanaka model.

Nanocomposites	PI-SiO_2	PI-SiO_2	PI-SiO_2	PI-SiO_2
Particle radius (Å)	6.29	8.50	11.56	13.45
Volume fraction (%)	3.41	4.78	6.14	4.34
Young's modulus of interphase (GPa)	10.53	8.3	7.83	7.84
Young's modulus of nanocomposites (GPa) (MD simulation)	4.52	4.34	4.37	4.24
Young's modulus of nanocomposites (GPa) (Effective interface model)	4.43	4.39	4.37	4.13
Young's modulus of nanocomposites (GPa) (Mori-Tanaka model)	3.93	4.04	4.15	4.01

RESULTS AND DISCUSSIONS

The modulus of the nanocomposites with four different sizes of nano-particles calculated from the molecular simulation and the effective interphase model are illustrated in Table 4. For the sake of comparison, the results calculated from the Mori–Tanaka model are also included in the Table 4. It was revealed that the modulus obtained using the effective interphase model is quite close to those obtained directly from the molecular simulation. However, the results calculated using the Mori–Tanaka model deviate from the molecular simulation, and the Mori–Tanaka results seem to underestimate the associate values. In addition, molecular simulation results indicate that when the particle sizes decrease, the corresponding modulus of the nanocomposites may increase if the particle volume fraction remains the same. In the molecular simulation, it is pretty difficult to have the molecular models with the same inclusion volume fraction because the volume fraction always varies and deviates from the initial set-up value. As can be seen from Table 4, the particle volume fractions are all different for the four cases after the molecular simulation even though they are the same at the beginning. Apparently, although the nanocomposites containing larger particles have the highest volume fraction, their modulus is almost the same as or even lower than the others with lower volume fraction of small particles.

In light of the fact that the small particle with more specific area can effectively enhance the stiffness of the nanocomposites, the applicability of the effective interphase model to characterize the size-dependent behaviors of the nanocomposites has to be examined. From the current simulations, the non-bonded gap varies between 3.2 and 4.0 Å, and thus for simplicity, we assume that the non-bonded gap is not influenced appreciably by the particle size, and its value is set equal to 3.6 Å for the following calculation. In addition, for the normalized non-bonded energy, because it is directly correlated to the degree of the non-bonded interaction, its relationship to the particle size was described using a power law as shown in Figure 8. With the properties of the normalized non-bonded energy and non-bonded gap, the modulus of the nanocomposites with various inclusion sizes was predicted using the effective interphase model. Figure 10 shows the predictions of the nanocomposites with volume fraction 4.2% using the effective interphase model. It can be seen that as the particle size increases, the modulus of the nanocomposites decreases accordingly. Moreover, the prediction eventually approaches the results of the Mori–Tanaka model as the particle size continues to increase. This tendency is similar to the results provided by Adrian et al. who performed the investigation on the size

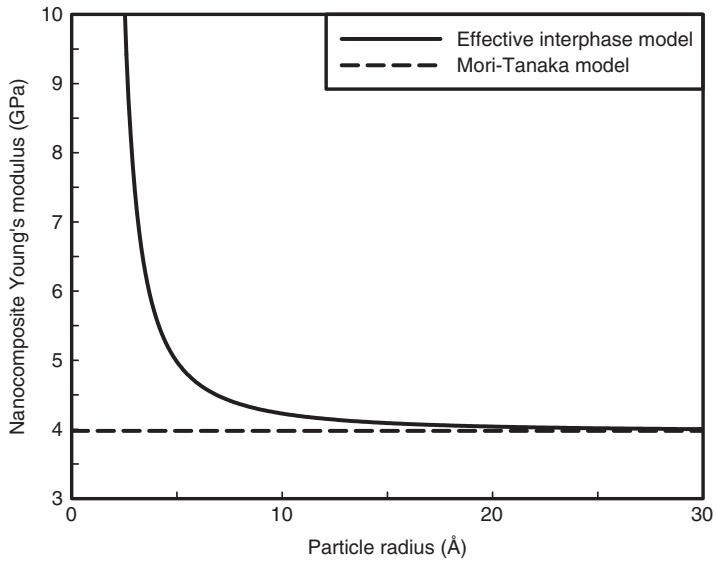

Figure 10. *Particulate size effect on the elastic modulus of silica/polyimide nanocomposites characterized suing effective interphase model.*

effect on elastic properties of bucky ball/polyethylene nanocomposites system using MD simulation [28].

CONCLUSIONS

The effective interphase model suitable for characterizing the elastic behaviors of particulate nanocomposites was proposed. The non-bonded gap as well as the non-bonded energy between the particulate inclusion and surrounding matrix were determined from the equilibrated molecular structures established through molecular simulation with minimum potential energy. With the properties of the effective interphase, the modulus of the nanocomposites was predicted from the continuum-effective interphase model. A comparison of the model predictions with the results calculated directly from molecular simulation reveals that the effective interphase model is able to characterize the properties of the particulate nanocomposites with accuracy. In addition, it was found that as the particle size decreases, the modulus of the nanocomposites increases consequently.

ACKNOWLEDGMENT

This research was supported by the National Science Council, Taiwan, under Contract No. NSC 94–2212-E-009–017 to National Chiao Tung University.

REFERENCES

1. Chen, B. and Sun, K. (2005). Poly (ε-caprolactone)/Hydroxyapatite Composites: Effects of Particle Size, Molecular Weight Distribution and Irradiation on Interfacial Interaction and Properties, *Polymer Testing*, **24**(1): 64–70.

2. Chisholm, N., Mahfuz, H., Rangari, V.K., Ashfaq, A. and Jeelani, S. (2005). Fabrication and Mechanical Characterization of Carbon/SiC-Epoxy Nanocomposites, *Composite Structures*, **67**(1): 115–124.
3. Vollenberg, P.H.T. and Heikens, D. (1989). Particle Size Dependence of the Young's Modulus of Filled Polymers: 1. Preliminary Experiments, *Polymer*, **30**(9): 1656–1662.
4. Vollenberg, P.H.T., de Haan, J.W., van de Van, L.J.M. and Heikens, D. (1989). Particle Size Dependence of the Young's Modulus of Filled Polymers: 2. Annealing and Solid-state Nuclear Magnetic Resonance Experiments, *Polymer*, **30**(9): 1663–1668.
5. Cho, J., Joshi, M.S. and Sun, C.T. (2006). Effect of Inclusion Size on Mechanical Properties of Polymeric Composites with Micro and Nano Particles, *Composite Science and Technology*, **66**(13): 1941–1952.
6. Ng, C.B., Ash, B.J., Schadler, L.S. and Siegel, R.W. (2001). A Study of the Mechanical and Permeability Properties of Nano- and Micron-TiO_2, Filled Epoxy Composites, *Advanced Composites Letters*, **10**(3): 101–111.
7. Reynaud, E., Jouen, T., Gauthier, C., Vigier, G. and Varlet, J. (2001). Nanofillers in Polymeric Matrix: A Study on Silica Reinforced PA6, *Polymer*, **42**(21): 8759–8768.
8. Jiang, L., Lam, Y.C., Tam, T.C., Chua, T.H., Sim, G.W. and Ang, L.S. (2005). Strengthening Acrylonitrile–Butadiene–Stryene (ABS) with Nano-Sized and Micron-Sized Calcium Carbonate, *Polymer*, **46**(1): 243–252.
9. Jordan, J., Jacob, K.I., Tannenbaum, R., Sharaf, M.A. and Jasiuk, I. (2005). Experimental Trends in Polymer Nanocomposites—A Review, *Materials Science and Engineering A*, **393**(1–2): 1–11.
10. Odegard, G.M., Clancy, T.C. and Gates, T.S. (2005). Modeling of the Mechanical Properties of Nanoparticle/Polymer Composites, *Polymer*, **46**(2): 553–562.
11. Cannillo, V., Bondioli, F., Lusvarghi, L., Montorsi, M., Avella, M., Errico, M.E. and Malinconico, M. (2006). Modeling of Ceramic Particles Filled Polymer-Matrix Nanocomposites, *Composites Science and Technology*, **66**(7–8): 1030–1037.
12. Avella, M., Bondioli, F., Cannillo, V., Errico, M.E., Ferrari, A.M., Focher, B., Malinconico, M., Manfredini, T. and Montorsi, M. (2004). Preparation, Characterisation and Computational Study of Poly (ε-caprolactone) Based Nanocomposites, *Materials Science and Technology*, **20**(10): 1340–1344.
13. Schmidt, D., Shah, D. and Giannelis, E.P. (2002). New Advances in Polymer/Layered Silicate Nanocomposites, *Current Opinion in Solid State and Materials Science*, **6**(3): 205–212.
14. Wang, H., Bai, Y., Liu, S., Wu, J. and Wong, C.P. (2002). Combined Effects of Silica Filler and Its Interface on Epoxy Resin, *Acta Materialia*, **50**(17): 4369–4377.
15. Wetzel, B., Haupert, F. and Zhang, M.Q. (2003). Epoxy Nanocomposites with High Mechanical and Tribological Performance, *Composites Science and Technology*, **63**(14): 2055–2067.
16. Laine, R.M., Choi, J. and Lee, I. (2001). Organic-Inorganic Nanocomposites with Completely Defined Interfacial Interactions, *Advanced Materials*, **13**(11): 800–803.
17. Ashby, M.F. and Jones, D.R. (1980). *Engineering Materials 1: An Introduction to Their Properties and Applications*, Pergamon Press, Oxford, UK.
18. Material Studio, Ver.4.0. Accelrys Inc., San Diego, CA.
19. http://www.accelrys.com/doc/materials/cerius40/compass/COMPASSTOC.doc
20. Nemat-Nasser, S. and Hori, M. (1993). *Micromechanics*: *Overall Properties of Heterogeneous Materials*, North-Holland-Amsterdam, London.
21. Hori, M. and Nemat-Nasser, S. (1993). Double-Inclusion Model and Overall Moduli of Multi-Phase Composites, *Mechanics of Materials*, **14**(3): 189–206.
22. Mori, T. and Tanaka, K. (1973). Average Stress in Matrix and Average Elastic Energy of Materials with Misfitting Inclusions, *Acta Metallurgica*, **21**(5): 571–574.
23. Eshelby, J.D. (1957). The Determination of the Elastic Field of an Ellipsoidal Inclusion and Related Problems, *Proceedings of the Royal Society of London. Series A*, **241**(1226): 376–396.
24. Toshio, M. (1982). *Micromechanics of Defects in Solids*, Martinus Nijhoff, The Hague.

25. Theodorou, D.N. and Suter, U.W. (1986). Atomistic Modeling of Mechanical Properties of Polymeric Glasses, *Macromolecules*, **19**(1): 139–154.
26. Allen, M.P. and Tildesley, D.J. (1987). *Computer Simulation of Liquids*, Clarendon Press, Oxford.
27. Shames, I.H. and Cozzarelli, F.A. (1992). *Elastic and Inelastic Stress Analysis*, Prentice-Hall, New Jersey.
28. Adrian, A., Sun, C.T. and Mahfuz, H. (2005). Effective of Particle Size Mechanical Properties of Polymer Nanocomposites, *Proceedings of the American Society for Composites the 20 Technical Conference*, Drexel University, Philadelphia, PA, September 7–9.